LETTERS

Common dependence on stress for the two fundamental laws of statistical seismology

Clément Narteau[1], Svetlana Byrdina[1,2], Peter Shebalin[1,3] & Danijel Schorlemmer[4]

Two of the long-standing relationships of statistical seismology are power laws: the Gutenberg–Richter relation[1] describing the earthquake frequency–magnitude distribution, and the Omori–Utsu law[2] characterizing the temporal decay of aftershock rate following a main shock. Recently, the effect of stress on the slope (the *b* value) of the earthquake frequency–magnitude distribution was determined[3] by investigations of the faulting-style dependence of the *b* value. In a similar manner, we study here aftershock sequences according to the faulting style of their main shocks. We show that the time delay before the onset of the power-law aftershock decay rate (the *c* value) is on average shorter for thrust main shocks than for normal fault earthquakes, taking intermediate values for strike-slip events. These similar dependences on the faulting style indicate that both of the fundamental power laws are governed by the state of stress. Focal mechanisms are known for only 2 per cent of aftershocks. Therefore, *c* and *b* values are independent estimates and can be used as new tools to infer the stress field, which remains difficult to measure directly.

The aftershock rate, Λ, is described by the Omori–Utsu law, $\Lambda(t) = k(t + c)^{-p}$, where t is the time from the main shock, k the productivity of the aftershock sequence, p the power-law exponent, and c the time delay before the onset of the power-law aftershock decay rate. The c value is strongly debated[4–10], as researchers[11,12] claim that c is close to zero and larger values are, at least partially, artefacts caused by lower data completeness after a main shock, especially during the main-shock coda. Investigations after the 2004 magnitude (M) 6.0 Parkfield, California, earthquake[13] and the 2004 $M = 6.6$ mid-Niigata Prefecture, Japan, earthquake[8] show that carefully identifying micro-earthquakes directly after main shocks give smaller but still non-zero estimates of the c value. We show for southern California and Japan that limiting the analysis to smaller main-shock and larger aftershock magnitudes results in non-zero c values that characterize a systematic behaviour of early aftershocks rather than a completeness artefact.

For southern California, we use an earthquake catalogue containing relocated events with focal mechanisms[14] from 1984 to 2003 and the Southern California Seismic Network (SCSN) catalogue since 2003. We select only high-quality events with a solution misfit <0.2 and a station distribution ratio ≥0.5. This subcatalogue contains more than 12,000 events. To identify main shocks, we adopt a time- and space-window algorithm[15,16] based on power-law relationships that reflect the hierarchical nature of the earthquake phenomenon (see Methods). The corresponding aftershocks with no focal mechanisms are extracted from the entire SCSN catalogue according to the same rules (>385,000 events between 1984 and 2007).

As for southern California, we use two different catalogues for Japan. We combine the F-Net catalogue with the JMA catalogue to isolate the focal mechanisms of main shocks since 1997 (F-Net) and

their respective aftershocks (JMA). To eliminate swarms of seismicity in the different volcanic areas of Japan, we also eliminate all aftershock sequences for which the geometric average of the times from their main shocks is larger than 4 hours. Thus, we remove spatial clusters of seismicity for which no clear aftershock decay rate exist.

In order to avoid artefacts arising from overlapping records, we focus on aftershock sequences produced by intermediate-magnitude main shocks, disregarding the large ones. For the same reason, we consider only the larger aftershocks and we stack them according to the main-shock time to compensate for the small number of events in each sequence. Practically, two ranges of magnitude have to be defined for main shocks and aftershocks, $\left[M_{min}^{M}, M_{max}^{M}\right]$ and $\left[M_{min}^{A}, M_{max}^{A}\right]$, respectively. We set the minimum magnitude thresholds for main shocks to $M_{min}^{M} = 2.5$ as this is the overall completeness level of the relocated catalogue[3]. Then, we determine that $M_{max}^{M} = 4.5$ is the main-shock magnitude from which overlapping records start to systematically influence the earthquake frequency–magnitude distribution of $M \geq 1.8$ aftershocks in the southern Californian catalogue (see Methods). The magnitude range of aftershocks, $\left[M_{min}^{A}, M_{max}^{A}\right]$, is a free parameter that may be varied to produce different estimates of the c value. In all cases, we select only aftershock sequences for which the local magnitude of completeness is smaller than M_{min}^{A}, the minimum magnitude threshold for aftershocks[17]. For each main shock, this completeness magnitude is calculated within a circle of 15 km radius over the three preceding years using a goodness-of-fit method[18]. Hence, the M_{min}^{A} value will not only determine the number of events that we consider in individual sequences but also the number of sequences that are taken into account (for example, taking $M_{min}^{A} = 2.4$ in southern California results in approximately 2,800 main shocks and more than 4,000 aftershocks during the first 12 hours).

The faulting style of main shocks is classified using rake angles, λ, in the Aki convention: $\lambda \approx 0°$ or $\lambda \approx \pm 180°$ for strike-slip events, $\lambda \approx 90°$ for thrust events, and $\lambda \approx -90°$ for normal events[3]. Here, we use both rake angles and a sliding window with a width of 60° and a step size of 5°. This results in 73 classes of main shocks. For each class and different intervals of magnitude, we stack aftershocks according to the time from their respective main shocks and we evaluate the c value by a maximum-likelihood method using continuous minimization by simulated annealing[4]. In addition, we evaluate the uncertainty of the maximum-likelihood estimates of the c value using a Monte Carlo approach and verify that all the observed behaviours are the same for the first and the second rake when they are treated independently. We also systematically perform a series of computations with different starting times of the optimization procedure to test the stability of the c value, and therefore eliminate potential artefacts related to catalogue incompleteness (see Methods).

For southern California, Fig. 1a, b shows the evolution of the c value with respect to the rake angle for aftershocks of magnitudes

[1]Institut de Physique du Globe de Paris (UMR 7154, CNRS, Univ. P7), 4 Place Jussieu, 75252 Paris Cedex 05, France. [2]Laboratoire de Géophysique Interne et Tectonophysique, UMR 5559, CNRS, Université de Savoie, IRD, 73376 Le Bourget-du-Lac Cedex, France. [3]International Institute of Earthquake Prediction Theory and Mathematical Geophysics, 84/32 Profsouznaya, Moscow 117997, Russia. [4]Department of Earth Sciences, University of Southern California, 3651 Trousdale Parkway, Los Angeles, California 90089, USA.
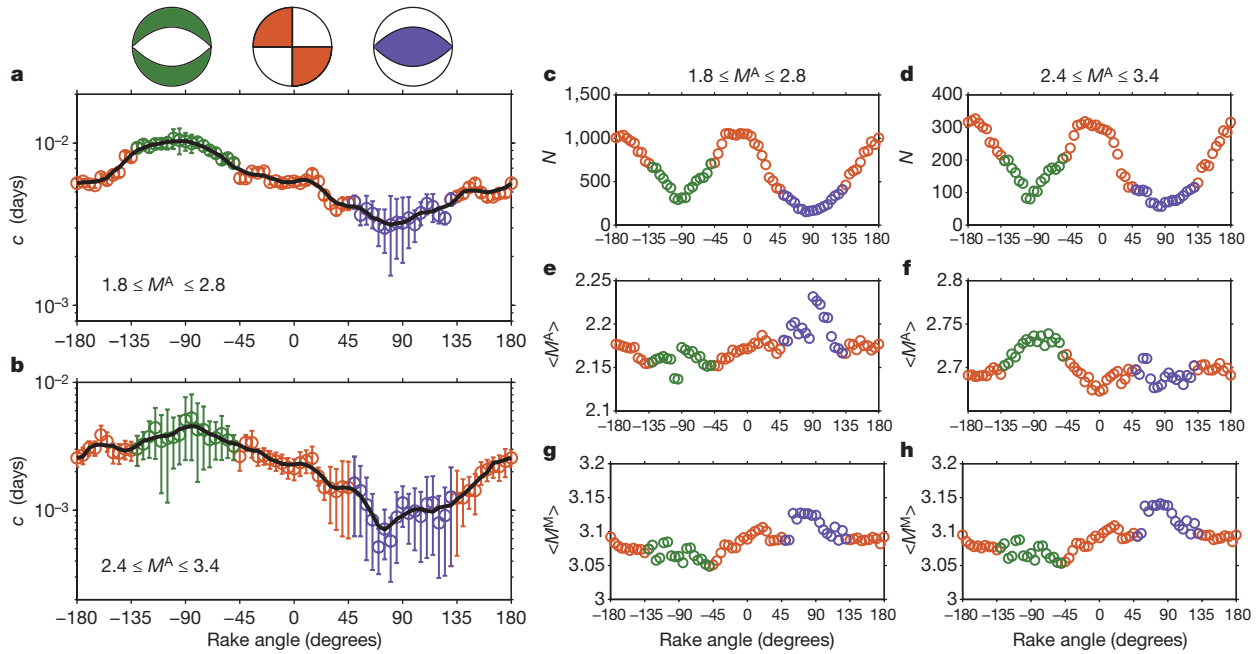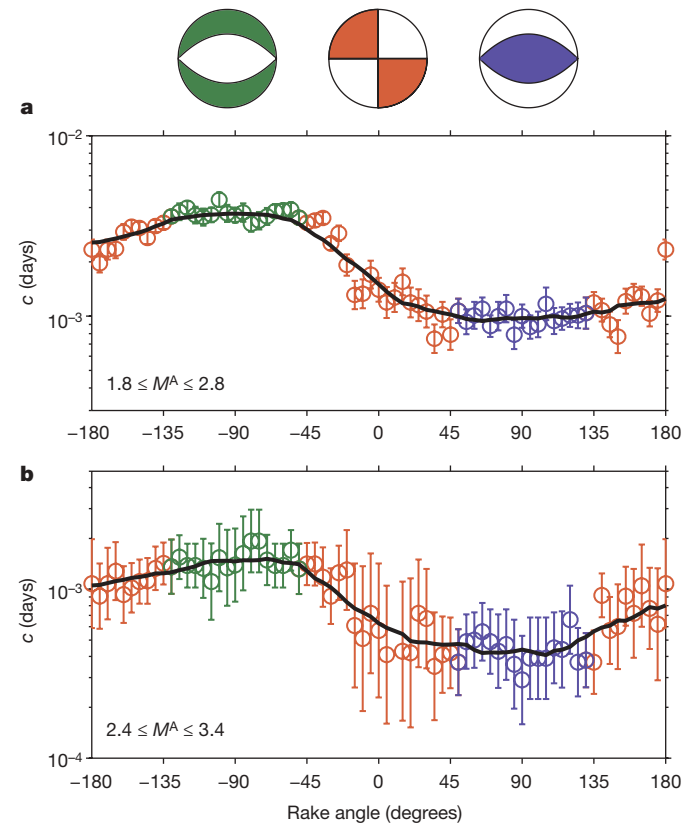
Figure 1 | Influence of faulting style on the time delay before the onset of the power-law aftershock decay rate in southern California. a, b, Logarithm of the c value with respect to rake angles for aftershock magnitude ranges of [1.8, 2.8] and [2.4, 3.4], respectively. Red, green and blue distinguish rake intervals of mainly strike-slip, normal and thrust events, respectively. Error bars are estimated by a Monte Carlo method and correspond to 16% and 84% quantiles of the maximum-likelihood estimates of c for 500 synthetic aftershock sequences at each point. **c–h**, Statistics of main shocks and aftershocks for both ranges of aftershocks. **c, d**, The number, N, of selected aftershocks. **e, f**, The average magnitude of selected aftershocks. **g, h**, The average magnitude of selected main shocks.

from 1.8 to 2.8 and from 2.4 to 3.4, respectively. For these intervals, Fig. 1c–h shows the numbers of selected aftershocks and the average magnitudes of selected main shocks and aftershocks for each rake angle. The uncertainty on the c value is strongly dependent on the number of events in the stack (Fig. 1c, d) but, even for high magnitude thresholds, a signal emerges. The c value for strike-slip earthquakes is higher than the c value for thrust earthquakes but lower than the c value for normal events. This means that the time delay before the onset of the power-law aftershock decay rate is shorter for thrust events, longer for normal ones and takes intermediate values for strike-slip events. The same behaviour is observed for the two magnitude ranges, despite a general shift in values that can be explained by a dependence of the c value on the average magnitude of aftershocks (see Methods). The differences of c values between thrust, strike-slip, and normal earthquakes cannot be explained by variations of the average magnitude of aftershocks (that is, the corresponding b value) because it does not exhibit a systematic pattern when plotted with respect to the rake angle (Fig. 1e, f). However, the average magnitude of main shocks reveals a similar behaviour for both magnitude ranges (Fig. 1g, h). Main shocks are larger for thrust earthquakes and smaller for normal earthquakes when compared to strike-slip events. This is a common feature in southern California that can be explained by differences in the earthquake frequency–magnitude distribution.

For Japan, to verify that missing aftershocks do not affect the estimation of c values, we also compare the completeness of the JMA catalogue with respect to the Peng catalogue[7] for 77 main shocks with magnitudes between 3.0 and 4.5 (see Supplementary Information). Then, as in southern California, we also found the same dependence of the c value on the rake angle for the same aftershock and main-shock magnitude ranges (Fig. 2a, b). Because the F-Net catalogue contains only few $M < 3.5$ events[3], the average magnitude of selected main shocks is higher than in southern California. As a result, the estimated c values are overall smaller.

In almost all cases, earthquake frequency–magnitude distributions follow a power-law relationship characterized by the b value, the exponent of the Gutenberg–Richter frequency–magnitude relation.

Figure 2 | Influence of faulting style on the time delay before the onset of the power-law aftershock decay rate in Japan. a, b, Logarithm of the c value with respect to rake angles of [1.8, 2.8] and [2.4, 3.4], respectively. From the comparison between the Peng[7] and the JMA catalogues, the optimization procedure starts 5×10^{-4} days after main shocks for $1.8 \le M^A \le 2.8$ aftershocks. Error bars are estimated by a Monte Carlo method and correspond to 16% and 84% quantiles of the maximum-likelihood estimates of c for 500 synthetic aftershock sequences at each point.

For the same catalogues that have been used to identify main shocks in Japan and southern California, the b value varies systematically for different styles of faulting. As shown in ref. 3, the b value for strike-slip events ($\sim 0.9 \pm 0.05$) is indeed higher than for thrust events ($\sim 0.7 \pm 0.05$) and lower than for normal events ($\sim 1.1 \pm 0.05$). Combining both observations, the c value and the b value exhibit a common dependence on focal mechanism that can be interpreted in terms of differential shear stress as follows.

The Mohr–Coulomb theory proposes that shear failure in a homogeneous medium subject to a uniform triaxial stress (σ_1, σ_2, σ_3) should occur on optimally oriented planes. These planes are parallel to the intermediate shear stress, σ_2, and form an angle Θ with σ_1, the maximum compressive stress. Then, the condition for faulting is governed by Amonton's law:

$$\tau \propto \mu \sigma_n$$

where μ is a coefficient of static friction, and σ_n and τ are the normal stress and the shear stress resolved on the fault surface. Assuming that one of the principal stresses is vertical and the other two lie in a horizontal plane, it is possible to express the angle Θ and the differential shear stress ($\sigma_1 - \sigma_3$) at which faulting may occur with respect to μ (ref. 19). In this context, the orientation of the principal shear stresses not only determines the faulting mechanism but also the amplitude of the differential shear stress. For example, the vertical stress corresponds to the maximum compressive stress for normal faulting and to the minimum compressive stress for thrust faulting. As a consequence, for the same coefficient of static friction, the differential shear stress should be much higher for thrust faulting than for normal faulting. Between these compressional and extensional regimes, strike-slip faulting should take an intermediate value of ($\sigma_1 - \sigma_3$). Hence, the relationship between the c value and the rake angle suggests that the time delay before the onset of the aftershock decay rate is positively correlated to the differential shear stress.

Considering that aftershocks result from a steplike perturbation of stress in the neighbourhood of a triggering event, various models for aftershock production predict that the amplitude of this perturbation controls the duration of the non-power-law regime of the aftershock decay rate over short time. See, for example, how an increasing stress step accelerates the onset of the power-law decay rate in rate-and-state friction models[20], in static fatigue models[4,21] and in damage mechanics models[22,23]. In addition, classical crack-growth experiments have shown that the amplitude of the stress perturbation is an increasing function of the remote applied stress[24]. The behaviour of the c value exposed in Figs 1a, b and 2a, b is an illustration of such relationships between the differential stress, the intensity of the stress redistribution and the shortness of the preliminary phase of an aftershock sequence. Nevertheless, there remains a high scatter in an individual aftershock sequence, most probably due to stress heterogeneity effects as well as measuring uncertainty. For this reason, the dependence of the c value on the differential shear stress can only be made through stacks of aftershocks.

The b value determines the ratio between the number of large and small earthquakes, and its variations can be associated with the ability of an earthquake rupture to propagate (lower b value) or not (higher b value) once nucleated. In this case, the positive correlation between the evolution of the c value and the b value across different stress regimes suggests a similar dependence on stress during earthquake propagation and aftershock production. Where the differential shear stress required to start sliding is higher, the porosity is reduced, stress interactions between the different parts of the fault zone are enhanced, and cracks can propagate faster in a wide range of directions[25,26]. Then, during the propagation of an earthquake, the characteristic time scales for failure, slip, or damage are shorter within process zones under higher confining stress. As a consequence, thrust earthquakes have a higher probability to propagate further than normal ones, consistent with the observation that the b value may be lower in a compressional regime than in an extensional one. If we assume that rupture terminates owing to structural and compositional heterogeneities, the same reasoning is again valid, and it takes a shorter time to nucleate aftershocks in higher-stress environments. As a result, the steady-state relaxation regime can be reached more rapidly and the c value is smaller for thrust earthquakes than for normal ones.

A common dependence on stress of earthquake frequency–magnitude distributions and aftershock decay rates offers new perspectives on earthquake-hazard analysis and earthquake physics, as it suggests that two independent aspects of seismicity can be used to constrain the state of stress in the brittle seismogenic crust. For example, the background seismicity and the quasi-systematic occurrence of aftershocks might be able to help in quantifying not only stress accumulation along major faults[27] but also the characteristic size of a potential earthquake[28].

METHODS SUMMARY

To identify main shocks, we deselect earthquakes of magnitude smaller than M which are within a $0.02 \times 10^{0.50M}$ kilometre radius circle during the first $0.125 \times 10^{0.55M}$ days after a magnitude M event[15,16]. Using the same spatial scaling, earthquakes that precede larger events by less than 12 hours are classified as potential foreshocks and removed from the catalogue of main shocks. This results in no overlapping aftershock sequences for the first 12 hours. For the selected main shocks, corresponding aftershocks with no rake angle are extracted from the entire SCSN catalogue ($>$385,000 events between 1984 and 2007) and the JMA catalogue ($>$1,100,000 events between 1997 and 2007). Practically, we select the smaller magnitude earthquakes occurring within 12 hours after a magnitude M main shock in a $0.02 \times 10^{0.50M}$ kilometre radius circle. Finally, only 2% of the selected aftershocks are also present in the catalogues of seismicity with focal mechanisms. Thus, data sets which are analysed here are different from the catalogues of seismicity that have been used to determine the relationship between the b value and the rake angle[3].

We investigate only earthquakes from particular magnitude ranges that can be shown to be complete even in early times of the aftershock sequence. The two major constraints are the following: (1) main shocks should be sufficiently small to have shorter coda waves such that subsequent aftershocks can be reliably detected; (2) aftershocks should be sufficiently big to ensure completeness at that particular magnitude level from the early times of an aftershock sequence. These magnitude ranges are determined from seismological and statistical constraints (see Methods).

Full Methods and any associated references are available in the online version of the paper at www.nature.com/nature.

1. Gutenberg, B. & Richter, C. F. Frequency of earthquakes in California. *Bull. Seismol. Soc. Am.* **34**, 185–188 (1944).
2. Utsu, T. Aftershocks and earthquake statistics. *J. Fac. Sci. Hokkaido Univ. Ser. VII* **3**, 379–441 (1965).
3. Schorlemmer, D., Wiemer, S. & Wyss, M. Variations in earthquake-size distribution across different stress regimes. *Nature* **437**, 539–542 (2005).
4. Narteau, C., Shebalin, P. & Holschneider, M. Temporal limits of the power law aftershock decay rate. *J. Geophys. Res.* **107**, B2359, doi:10.1029/2002JB001868 (2002).
5. Shcherbakov, R., Turcotte, D. L. & Rundle, J. B. A generalized Omori's law for earthquake aftershock decay. *Geophys. Res. Lett.* **31**, L11613, doi:10.1029/2004GL019808 (2004).
6. Vidale, J. E., Peng, Z. & Ishii, M. Anomalous aftershock decay rates in the first hundred seconds revealed from the Hi-net borehole data. *Eos Trans. AGU* **85** (Fall Meet. Suppl.), abstr. S23C-07 (2004).
7. Peng, Z. G., Vidale, J. E., Ishii, M. & Helmstetter, A. Seismicity rate immediately before and after main shock rupture from high frequency waveforms in Japan. *J. Geophys. Res.* **112**, B03306, doi:10.1029/2006JB004386 (2007).
8. Enescu, B., Mori, J. & Miyazawa, M. Quantifying early aftershock activity of the 2004 mid-Niigata Prefecture earthquake (M_w6.6). *J. Geophys. Res.* **112**, B04310, doi:10.1029/2006JB004629 (2007).
9. Nanjo, K. Z. Decay of aftershock activity for Japanese earthquakes. *J. Geophys. Res.* **112**, B08309, doi:10.1029/2006JB004754 (2007).
10. Kilb, D., Martynov, V. & Vernon, F. Aftershock detection as a function of time: results from the ANZA seismic network following the 31 October 2001 M_L 5.1 Anza, California, earthquake. *Bull. Seismol. Soc. Am.* **97**, 780–792 (2007).
11. Kagan, Y. Y. Short-term properties of earthquake catalogs and models of earthquake source. *Bull. Seismol. Soc. Am.* **94**, 1207–1228 (2004).

12. Lolli, B. & Gasperini, P. Comparing different models of aftershock rate decay: the role of catalog incompleteness in the first times after main shock. *Tectonophysics* **423,** 43–59 (2006).

13. Peng, Z. G., Vidale, J. E. & Houston, H. Anomalous early aftershock decay rate of the 2004 M_w 6.0 Parkfield, California, earthquake. *Geophys. Res. Lett.* **33,** doi:10.1029/2006GL026744 (2006).

14. Hauksson, E. Crustal structure and seismicity distribution adjacent to the Pacific and North America plate boundary in southern California. *J. Geophys. Res.* **105,** 13875–13903 (2000).

15. Gardner, J. & Knopoff, L. Is the sequence of earthquakes in southern California with aftershocks removed Poissonian? *Bull. Seismol. Soc. Am.* **5,** 1363–1367 (1974).

16. Reasenberg, P. Second-order moment of central California seismicity, 1969–1982. *J. Geophys. Res.* **90,** 5479–5495 (1985).

17. Schorlemmer, D. & Woessner, J. Probability of detecting an earthquake. *Bull. Seismol. Soc. Am.* **98,** 2103–2117 (2008).

18. Wiemer, S. & Wyss, M. Minimum magnitude of completeness in earthquake catalogs: examples from Alaska, the western United States, and Japan. *Bull. Seismol. Soc. Am.* **90,** 859–869 (2000).

19. Sibson, R. H. Frictional constraints on thrusts, wrench and normal faults. *Nature* **249,** 542–544 (1974).

20. Dieterich, J. A constitutive law for rate of earthquake production and its application to earthquake clustering. *J. Geophys. Res.* **99,** 2601–2618 (1994).

21. Scholz, C. Microfractures, aftershocks, and seismicity. *Bull. Seismol. Soc. Am.* **58,** 1117–1130 (1968).

22. Shcherbakov, R. & Turcotte, D. L. A damage mechanics model for aftershocks. *Pure Appl. Geophys.* **161,** 2379–2391 (2004).

23. Ben-Zion, Y. & Lyakhovsky, V. Analysis of aftershocks in a lithospheric model with seismogenic zone governed by damage rheology. *Geophys. J. Int.* **165,** 197–210 (2006).

24. Atkinson, B. K. Subcritical crack growth in geological materials. *J. Geophys. Res.* **89,** 4077–4114 (1984).

25. Amitrano, D. Brittle-ductile transition and associated seismicity: experimental and numerical studies and relationship with the *b*-value. *J. Geophys. Res. B* **108,** 2044, doi:10.1029/2001JB000680 (2003).

26. O'Connell, D. R. H., Ma, S. & Archuleta, R. J. Influence of dip and velocity heterogeneity on reverse- and normal-faulting rupture dynamics and near-fault ground motions. *Bull. Seismol. Soc. Am.* **97,** 1970–1989 (2007).

27. Narteau, C., Shebalin, P. & Holschneider, M. Loading rates in California inferred from aftershocks. *Nonlin. Process. Geophys.* **15,** 245–263 (2008).

28. Schorlemmer, D. & Wiemer, S. Microseismicity data forecast rupture area. *Nature* **434,** 1086 (2005).

METHODS

The selection of main shock-aftershock sequences requires four parameters: two for the aftershock magnitude range $\left[M_{min}^{A}, M_{max}^{A}\right]$; one for the radius of influence of individual main shock, R; and one for the maximum main-shock magnitude, M_{max}^{M}. These parameter values are determined from seismological and statistical constraints. The radius R has to be as small as possible in order to limit the perturbations due to seismic noise, but large enough to capture a significant number of aftershocks within the first day. Practically, we take $R = 0.02$ km according to the relationship between the magnitude and the rupture length[29]. The lower aftershock magnitude threshold $M_{min}^{A} = 1.8$ is given by catalogue completeness[17] in southern California. The higher magnitude threshold M_{max}^{A} is given from the M_{min}^{A} value using a constant magnitude interval, Δ, determined according to the number of aftershocks in the catalogue. Because the results depend on the aftershock magnitude range, it is always better to take the Δ value as small as possible (here $\Delta = 1$). To determine M_{max}^{M}, we analyse one single magnitude range of aftershocks from 1.8 to 2.5 in southern California. Classes of main shocks are formed using a sliding window of width 0.5 that moves in 0.1 unit steps from M_{min}^{M} to 5.3. For each class, we generate the corresponding list of aftershocks, and estimate $<M^{A}>$, the average magnitude of these aftershocks (Supplementary Fig. 1). For an increasing main-shock magnitude, the $<M^{A}>$ value is generally increasing if $M^{M} > 4.5$ because smaller aftershocks are increasingly missing in the stacks. Below this threshold, the value of $<M^{A}>$ oscillates around an equilibrium value, indicating that the impact of overlapping records on catalogue completeness is stationary; therefore, we set $M_{max}^{M} = 4.5$.

Without distinction of faulting style, we evaluate the c value separately for different magnitude ranges of aftershocks. Thus, we observe that the characteristic time before the power-law decay starts is continuously decreasing as the average magnitude of aftershocks is increasing (Supplementary Fig. 2). A similar relationship has been reported for individual earthquakes in California and Japan[5,9]. These observations explain the changes in mean c values for different aftershock magnitude ranges in Figs 1a, b and 2a, b (see also Supplementary Figs 9 and 10). Then, absolute variations of the mean c value can be entirely separated from the dependence of the c value on the rake angle.

For the maximum-likelihood estimates of c, the optimization procedure depends on two values: T_{comp}, the time at which the catalogue is complete (that is, all aftershocks are recorded), and T_{start}, the time at which we start the fit. It is evident that if $c < T_{comp}$, the estimated c value cannot be considered as reliable. In the case $c < T_{start}$, the error on the c value is large and increases exponentially with T_{start}. In the case $T_{start} < T_{comp} < c$, the c value may be overestimated because of catalogue incompleteness. Therefore, the preferred condition for the estimation of the c value is $T_{comp} < T_{start} < c$.

For Japan, we take advantage of a hand-picked catalogue[7] to determine values of c and T_{comp} that are not affected by missing aftershocks. For different aftershock magnitude ranges, we verify that $c > T_{comp}$. Then, using the events listed in the JMA catalogue, we can use an increasing T_{start} value to converge towards a good estimation of the c values (that is, the c values obtained from the hand-picked catalogue). This convergence depends on the proportion of recorded events (see Supplementary Table 1, and Supplementary Fig. 7a–c) but also on their distribution over time (see Supplementary Fig. 4). For $2.4 \leq M^{A} \leq 3.4$ aftershocks, we show that the JMA catalogue can be considered complete and we can take a very small value of T_{start}. For $1.8 \leq M^{A} \leq 2.8$ aftershocks, it is recommended to take $T_{start} = 5 \times 10^{-4}$ day because this is the time at which the proportion of recorded events switches rapidly from 0 to 1 (see Supplementary Fig. 4). Then, for these events also, the c value is larger for normal events, smaller for thrust events, and takes intermediate values for strike-slip events (Fig. 2a).

Most importantly, for any aftershock catalogue for which the level of completeness is not well defined, it is possible to use the starting time of the optimization procedure to estimate the stability of the c value and verify that missing aftershocks do not perturb the estimation of this parameter. In the present study, we perform such an analysis for southern California (Supplementary Fig. 8). We show that for $T_{start} = 10^{-4}$ days (9 s), $T_{start} = 5 \times 10^{-4}$ days (45 s), $T_{start} = 10 \times 10^{-4}$ days (90 s) and $T_{start} = 14 \times 10^{-4}$ days (2 min) there is no significant change in the estimation of c values for all classes of rake angles. As the catalogue of $M^{A} \geq 1.8$ aftershocks is complete 2 min after a $M^{M} < 4.5$ main shock[10], this stability in the c value clearly indicates that the missing aftershocks do not affect the estimation of this parameter in this particular case (that is, $T_{comp} < T_{start} < c$ for all considered parameters, including different rake angles).

29. Wells, D. L. & Coppersmith, K. J. New empirical relationships among magnitude, rupture length, rupture width, rupture area and surface displacement. *Bull. Seismol. Soc. Am.* **84**, 974–1002 (1994).